IN-24
372-742

An Insidious Mode of Oxidative Degradation in a SiC-SiC Composite

Linus U.J.T. Ogbuji
NASA Lewis Research Center
Cleveland, OH 44135

Abstract

The oxidative durability of a SiC-SiC composite with Hi-Nicalon fiber and BN interphase was investigated at 800°C (where pesting is known to occur in SiC-SiC composites) for exposure durations of up to 500 hours and in a variety of oxidant mixes and flow rates, ranging from quasi-stagnant room air, through slow flowing O_2 containing 30-90% H_2O, to the high-velocity flame of a burner rig. Degradation of the composite was determined from residual strength and fracture strain in post-exposure mechanical tests and correlated with microstructural evidence of damage to fiber and interphase. The severest degradation of composite behavior was found to occur in the burner rig, and is shown to be connected with the high oxidant velocity and substantial moisture content, as well as a thin sublayer of carbon indicated to form between fiber and interphase during composite processing

1.0 Introduction

The primary role envisaged for non-oxide ceramic-matrix composites (CMCs) is in the hottest sections of advanced aircraft engines and land turbines, such as combustor liners and jet-exhaust vanes. In those applications the components will be subject to attack by fast streams of very hot and corrosive products of combustion. Therefore, the integrity and durability of components in such aggressive environments are a major concern as

possible determinants of engine lifetimes. This is especially true of the material at the fiber-matrix interphase of CMCs (hence called the *interphase*) which serves as a compliant layer to enhance load transfer as well as a debond layer to ensure graceful composite failure. The most prominent and perhaps most advanced CMC is the SiC-SiC composite which features (typically) SiC fiber reinforcement in a SiC matrix, separated by a BN interphase layer. The BN interphase remains the weakest link in the composite, both mechanically speaking and in terms of resistance to oxidative and hydrolytic degradation in the sort of environment expected in a turbine engine. NASA has an interest in the development of interphases for high-temperature non-oxide CMCs, and, at the Lewis Research Center, a large effort is devoted to assessing and improving the performance of the BN interphase in SiC-SiC composites under a variety of service-related conditions.

BN ordinarily oxidizes to a condensed phase, B_2O_3; this makes it superior to carbon for use as an interphase material (as the oxidation of carbon leaves no condensed residue). Nevertheless, there remain significant problems connected with the oxidation and loss of BN, especially when it is in contact with siliceous material. BN oxidizes to boria, B_2O_3, which is liquid above 410°C.[1] and will dissolve SiC to form a borosilicate that stays liquid down to the eutectic temperature of 372°C.[1,2] This is deleterious for two reasons. Firstly, dissolution of the fiber in a SiC-SiC composite weakens the fiber through reduction of cross-section, flaw initiation, and creation of stress-concentration raisers. Secondly, in the presence of water vapor boron is volatilized from the borosilicate and lost as gaseous hydroxide.[3,4] This process eventually leaves SiO_2 glass where the BN had been. The glass can cement fiber to matrix or to adjacent fiber, thus rigidifying the composite and creating

further stress concentration.[5] Since H_2O is a substantial product of hydrocarbon combustion and always present in an engine ambient, the possibility of quick loss of the BN interphase has become an issue of major concern. If exposed to the ambient through matrix cracking, the interphase can be quickly consumed and replaced with cementitious glass that embrittles and weakens the composite. This mode of degradation, known as *pesting*, is prevalent at the intermediate regime of temperatures below which the interphase oxidation is too slow, and above which rapid formation of surface silica protects the interphase by sealing off the ambient.

A similar pesting behavior has been reported for composites with SiC fibers, magnesium aluminosilicate (MAS) or alumina matrix, and carbon or BN interphase between ~500 and 900oC.[6,7] In these composites pesting degradation is also characterized by the formation of silica where the interphase used to be. Studies performed at 750[8] and 800-900°C[8-10] have demonstrated the phenomenon of pesting in MAS/SiC and SiC/SiC composites, respectively.

It is reasonable to assume that these oxidative/hydrolytic degradation processes start at the surface of a sample, where cracks initiate and initial contact is made with the ambient. In most cases this is borne out by observation. Results in our laboratories[11] show that, in most cases, a damage front starts at the surface and advances one tow at a time towards the interior of the material (Fig. 1). Accordingly, it has been assumed that the progress of that front can be characterized by micrography and the extent of damage quantified by measuring the amount of load-bearing cross-section of the sample lost. Models for

quantifying the extent of damage are based on this "progressive" view of the degradation process. Evans and co-workers[8] have shown that, in MAS-SiC composites the stress at which a test sample fails after pesting exposure correlates with the residual cross-sectional area of the sample which is supposedly free of damage and is still characterized by fibrous failure. Morsher[10] has established a similar correlation in SiC-SiC composites by using measured recession distances of the BN interphase from exposed fiber ends as an index of the extent of damage.

When the extent of damage so determined and quantified can be correlated with the prevailing factors of degradation in the environment (temperatures, oxidant partial pressures, moisture content and flow velocities, etc.), the usefulness of that approach in modelling and predicting the service lifetimes of CMC components becomes evident. However, that predictive capability would be lost in a situation where damage did not progress predictably (measurably) from the sample surface to its interior. Such a situation has been observed for SiC-SiC composites with Hi-Nicalon™ fibers, BN interphase, and a matrix of melt-infiltrated (MI) SiC, when tested at 800°C in a fast-flame burner rig. In that observation, presented in this paper, the residual strength of the Hi-Nicalon/BN/MI-SiC composite declined by more than half after 150-hour exposures at 800°C in the fast flame of a burner rig with a moisture content of ~10%, and its toughness (indicated by strain to failure) decreased by an order of magnitude. In contrast, the same material remained essentially unimpaired after exposures of similar duration in static or slow-flowing oxidants with higher moisture contents.

The burner rig facilities at the NASA Lewis Research Center were designed to simulate the combustion environments of turbine engines,[12] complete with high-velocity flame and the usual mix of combustion products including, water vapor which inevitably constitutes about 10% of the oxidation products of Jet-A fuel.[13] The low-pressure burner rig used in this investigation operates at 1.0 atm. and has the capability for tensile loading of specimens during oxidation, and operates at Mach 0.3 flame velocities, which is in the range of tens of meters per second expected in service.

2.0 Experimental Procedure

2.1 Material

The composite materials used in this investigation were supplied by Carborundum and consisted of 8-ply lay-up of plain-weave Hi-Nicalon tows with an interphase of chemical-vapor-infiltrated (CVI) BN in a matrix of melt-infiltrated (MI) SiC. In this material the 0.58μm interphase layer around each fiber is separated from the matrix by a cladding of CVI SiC ~1.0μm thick, to protect the interphase during matrix processing. (These are nominal thicknesses, assuming a uniform dispersion of all constituents.) The samples were supplied as tensile test bars 152 mm x 12 mm x 2 mm (6" x 0.5" x 0.08"), machined into a dog-bone shape, with fiber ends exposed along the cut thin edge. The bars were tested under the conditions summarized in Table 1.

2.2 Oxidation

Three oxidation environments were investigated: an open, static system (box furnace), an open dynamic system (burner rig), and a closed system (tube furnace). The suitability of the burner rig for simulating overall engine combustor ambient has been stated above. The advantage of a tube furnace was that oxidant mix and (to a lesser extent, its flow rate) could be varied as desired, to simulate expected moisture content in relevant segments of a turbine combustor liner. All oxidation in this study was performed at 800°C. While exact temperature control was not critical, care was taken to ensure uniform temperature over the sample gage zone. For the burner rig it was ascertained by optical pyrometry that no part of the flame was more than 4°C above or below the set temperature of 800°C; for the tube furnace, the temperature profile determined with the aid of thermocouples showed that the middle 4-inch segment of the test bar was at 800°C; the box furnace had a more varied temperature profile, hence the bars were placed directly below the thermocouple.

Some sample bars were oxidized in the box furnace, in room air with relative humidity ranging from 40% to 98% over the 20-days of oxidation; others were oxidized in a horizontal tube furnace with a regulated mix of oxygen and distilled-deionized water in proportions ranging up to 90% moisture content; and yet others in the atmospheric-pressure burner rig in which the H_2O content was fixed at ~10% by the stoichiometric combustion of Jet-A fuel in air. The box furnace ambient was essentially static; the tube furnace oxidant mix flowed at 500 sccm in the 2-inch furnace tube, giving a linear flow velocity of ~0.5 cm/sec; while the burner rig flame impinged on the test bars at 228 mph (Mach 0.3), or 100 meters per sec. Sample placement in the burner rig flame was varied so

that the flame impinged directly on the exposed fiber ends at the cut edge of the sample in most cases, and in some cases on the broad face of the sample which was sealed with dense SiC and provided no access to the interphase. This was done in order to examine the possible effect of crack orientation (relative to flowing oxidants) on interphase degradation by the ambient.

As mentioned earlier, the samples used in this study had fiber ends exposed along their machined edges to produce a worst-case scenario of oxidant access. In the follow-up study now underway the exposed edges are sealed with dense SiC; controlled flaws are introduced by pre-cracking the bars; and a nominal tensile stress of 50 MPa is applied to keep the cracks open. This level of stress is considered high enough to wedge open pre-existing cracks. However, it is too low to initiate matrix cracks, since accoustic emission couplings revealed that the first cracking occurred around 90 MPa during the mechanical testing of as-received material. To make the exposure conditions comparable in the two studies, the same 50MPa stress was applied to some burner rig bars in the study reported here (Samples 8 and 9). No samples failed in the burner rig under the 50MPa nominal stress. Nevertheless, Sample 10 was tested in the burner rig without stress, to ascertain whether the nominal stress influenced degradation rate in the present study.

2.3 Testing and Examination

After oxidation exposure the bars were subjected to mechanical tests and their stress-strain behaviors recorded, as shown in Table 1. The main results sought from the mechanical tests were the residual values of the ultimate tensile strength, σ_u, and strain to failure, ε_f.

In the box furnace and tube furnace the entire sample was exposed to the oxidants at the chosen temperature; accordingly, degradation should not be localized in these samples. In contrast, the burner rig samples were oxidized only in the 1-inch flame zone at the center of the bar, which also coincided with the gage zone in the tensile test. Hence, the burner rig samples were expected to fail inside that one-inch zone of degradation. Where that did not occur (Sample #8, Table 1), the values of σ_u and ε_f were still retained as indicating a lower bound for the strength and failure strain of the degraded zone.

To determine the microstructural changes underlying any strength degradation observed, the broken samples were examined by SEM, both on the surfaces exposed by fracture and on surfaces exposed elsewhere in the degraded zone by sectioning and polishing. Burner rig bars that failed outside the flame zone were re-tested to induce fracture within the flame zone for fractography. The main features determined by SEM were the integrity of the interphase around fibers in the zone of degradation and failure: continuity of the BN interphase, and evidence of its replacement with glass. This was done by both micrography and EDS, with the microscope operating in the range of 2 to 5.0 KeV in the EDS analysis for boron.

3.0 Results

(1) The residual strengths and fracture strains of the SiC-SiC samples appear in Table 1, and the residual strengths are also shown charted in Figure 2. The relevant exposures of the samples are summarized in Table 1.

The differences of treatment or placement between the 4 burner rig samples is indicated in Table 1. A plot of the failure strains, not shown, was essentially identical to Figure 2. It is also clear from Table 1 that the trend of ε_f exactly parallels the trend of σ_u. The agreement between those two trends lends confidence to our intepretation of degradation effects in these materials. Clearly, the results fall into two categories. In the first category are the ultimate tensile strengths of the first eight samples, which are essentially the same and well within 15% of the as-received strength (of Sample 1). In the second category are the samples exposed in the burner rig (last four samples in Figure 2), which failed at 30-40% of the as-received strength. In other words, the material retained its strength after every furnace oxidation, but exhibited a dramatic drop in strength and fracture strain (60% and 90%, respectively) after a burner rig exposure.

It is apparent from Table 1 and Figure 2 that the role of H_2O content of the oxidizing ambient in promoting degradation is not straight-forward. This is clearer in Fig. 3 where residual strength is shown against moisture content. The sharp dip for the three burner rig samples (at 10% moisture content) and the apparent lack of a trend for the other samples clearly indicate an anomaly which is not attributable to moisture content alone. The trends indicate that, in the furnace oxidation exposures, the effect of increasing moisture content is minimal, while, in the burner rig, some other factor is contributing more than moisture content to the degradation. The close agreement in the results for all burner rig samples suggest that the factors that were varied in the rig (sample orientation the presence or absence of a nominal stress) had no significant impact on the degradation. We note, also,

that it was not possible to vary moisture content in the burner rig since, as we have seen, burner rig moisture content is determined by the combustion chemistry. Therefore, the results of this study do not show whether or not the extent of damage scales with moisture content in the burner rig. What it does show is that moisture content alone plays a minor role in Hi-Nic/BN/SiC degradation, compared with some other factor in the burner rig.

Figure 4 shows fracture surfaces of the material after the most severe exposures in the tube furnace: (a) 500 hours in 30% H_2O+70% O_2, and (b) 150 hours in 90% H_2O+10% O_2. The main result to note in these micrographs is very the fibrous nature of the failure. Minor evidence of degradation was limited to those tows that intersect the exposed edges of the samples. This agrees with the indication in Figure 2 that there was minimal loss of mechanical properties in samples oxidized in the furnaces. In contrast, Figures 5 was from a burner rig sample and illustrates the flat and brittle fracture observed in all such samples, in agreement with the result in Figure 2 indicating a severe loss of mechanical properties in these samples.

4.0 Discussion

4.1 The Results

Figures 2 and 3 are not to be interpreted to mean that this material is strongly resistant to degradation by moisture. They merely show that, under the conditions investigated here, especially the rather short times, the effect of moisture is not as pronounced as some other effects we shall highlight shortly. (It is probable that, under the static-to-slow oxidant flow conditions in a furnace, 500 hours is too short a duration for moisture effects to become

manifest.) That leaves flame speed as the most probable factor affecting the mechanical properties of the composites, and indicates that a very high oxidant velocity is a more deleterious factor of composite degradation than moisture content alone. Note that flow rate in the burner rig oxidant is 4 orders of magnitude higher than in the tube furnace (and more representative of actual flow rates expected in service).

Several microstructural features distinguish the degradation mode in the burner rig from that in the furnaces. Figure 5(b) shows an important feature which was observed on all fracture or polished surfaces of the burner rig samples: A close inspection reveals a pair of pin holes wherever adjacent fibers are close enough together for a neck to form between them. The pin holes turned out to be reliable indicators of substantial degradation of the interphase. The necks are shown at higher magnification in Figures 6(a) and (b). Close examination of Figure 6(a) shows the beginning of a sublayer of glass (arrowed) between the fiber and interphase; in many cases the now glassy interphase was found to extend entirely across the gap between fibers, leaving no indication of the original BN layers. The arrows in Figure 6(b) point to crack fronts emanating from the degraded segment of interphase between pin holes. They indicate that fiber failure intiated in the points of fiber contact with the now glassy interphase.

Another important piece of information obtained in the vicinity of the pin holes is evidence of interphase reaction. Figure 7(a) is the EDS spectrum taken from an intact segment of an interphase; it features a nitrogen peak, and a boron peak (as a prominent shoulder to the carbon peak), but no evidence of oxygen. In contrast, Figure 7(b) is representative of the

spectra obtained from segments of interphase around and between pin holes; it features a very prominent oxygen peak, but no nitrogen or boron. (The Si peaks are not shown in Figures 7.) There is a minor shift in peak positions at the low energy end due to instrument error, and the spectra look a bit bumpy as no smoothing has been applied, but the features of importance are well delineated. Fig. 7(b) indicates clearly that the segment of interphase which lies between the holes has been replaced by silica glass.

It is significant that pin holes, boron depletion zones, and fiber fracture initiation sites, all tell-tale signs of interphase degradation, were observed for every fiber across the fracture surfaces of every sample exposed in the burner rig for longer than ~100 hours at 800°C. The pin holes must represent cross-sections through tubes or bubbles that formed in the interphase, and their formation is connected with the mechanism of interphase reaction and degradation.

4.2 Interphase Reactions

The end product of interphase degradation is, as we have seen, silica glass. Yet this SiO_2 could not have resulted from direct oxidation of any SiC component in the vicinity of the interphase. At 900°C, the lowest temperature for which reliable data exist in the literature for SiC oxidation, the fastest oxide growth rate determined for CVI SiC is a barely measurable ~5 nm/min;[14] at 800°C the oxidation rate must be negligible. In contrast, 800°C is quite a high temperature for the oxidation of BN according to the equation:

$$2BN(s) + 3/2O_2(g) = B_2O_3(l) + N_2(g) \quad (1)$$

The resulting oxide is liquid at 800°C (being solid only below ~410°C, as we have seen). Phase diagrams for the SiO_2-B_2O_3 system show that liquid boria will dissolve its own weight of SiO_2 at 800°C to form borosilicate liquid[1,2] and recent results show that liquid boria will also dissolve large amounts of SiC[3] (although the exact limits of solubility between SiC and B_2O_3 remains to be determined). The liquid boria formed by reaction (1) will dissolve its retaining walls of SiC fiber and SiC cladding to form a viscous borosilicate liquid in the following reaction:

$$B_2O_3(l) + SiC(s) \rightarrow B_2O_3\text{-}SiO_2(l) + CO(g) \quad (2)$$

The borosilicate liquid most probably also attains equilibrium (through dissolution) with the BN interphase in contact with it, thereby releasing NO or N_2 in a reaction analogous to eq. (2), but this introduces no new element into the process described here. The main point here is that the BN interphase at the reaction location has been replaced with a borosilicate liquid.

The next step in the reaction process has been examined in some detail by Jacobson and co-workers.[3,4] Boria and borosilicates are strongly hydrophylic[2] and in the liquid form rapidly hydrolyzed, even in air where the moisture content is only a few ppm.[3,4] The hydrolysis reaction liberates gaseous boron hydroxides (HBO_2 and H_3BO_3 as identified by mass spectrometry[4]). With the consequent loss of boron from the borosilicate liquid, its

viscosity increases until it is transformed into solid silica glass. The removal of boron from the interphase reaction zone is so thorough that SEM/EDS examination usually shows the resulting oxide to be eventually free of boron, especially closer to the sample surface.[9,10] Therefore, without a careful analysis it is possible to overlook the transition involved. In careful experiments on the oxidation of SiC/BN/SiC minicomposite (described as a tow of BN-coated Hi-Nicalon fiber infiltrated with a CVI SiC sheath) in moist air, Morscher et al.[10] observed compositional changes in the interphase: from BN in the sample interior (evidenced in strong N signal with no O signal), through a transition zone of borosilicate (decreasing N signal and increasing O signal), to silica at the sample surface.

Sun and co-workers[15,16] have reported similar observations on an analogous composite of barium magnesium alimonosilicate (BMAS) glass reinforced with dual-coated Nicalon™ (SiC) fibers with the dual coating consisting, as in our case, of a BN interphase overcoated with a protective SiC layer. They report that, when the material is tested in static fatigue at 600°C, degradation started with consumption of the BN/fiber interphase which is replaced by amorphous silica copiously riddled voids. However, they thought that the silica resulted from direct oxidation of the fiber, and based this argument on thermodynamic calculations which show that, ***at very low oxygen partial pressures***, SiC oxidation is triggered before BN oxidation.[17] The mechanism they proposed for the reactions leading to degradation differs from that given here. The difference is a matter of whether the degradation starts with oxidation of the fiber or of the interphase. While thermodynamics may predict that SiC will getter oxygen from BN at very low oxygen partial pressures, there are two important caveats: In the first place, it is questionable whether the oxygen partial pressures

at an exposed interphase is in the very low regime assumed in those thermodynamic calculations.[17] We note that in our study (oxidation in a flame) and probably in theirs also (static fatigue in air) the BN interphase is exposed to ambient oxidants at atmospheric pressure – by machining in our case and presumably by cracks in their case. Secondly, Sun et al. show (in Fig. 4(B) of their report)[15] that the ~0.5μm BN interphase was totally converted to (highly porous) silica after 32 hours at 600°C. Such a phenomenal silica growth rate that is not supported by the kinetics of SiC oxidation, which show that only a negligible monolayer or so of oxide will grow on SiC in 1.0 atm. of air below ~900°C.[14] This implies that formation of silica by direct oxidation of SiC in their experiment is ruled out, and the indirect route (via boria and borosilicate) is indicated.

4.3 Degradation Mechanism

The foregoing explains the origin of the silica bridges identified in Figures 5 and 6 above, and which are thought to embrittle our samples by cementition of fibers. The fact that this embrittling silica bridge is apparently formed everywhere at once in the flame zone of our burner rig samples requires explanation. Clearly, the reaction processes must be creating a pathway for the deep penetration of the amibient into our samples, and the process that generates this pathway must be peculiar to our combination of Hi-Nicalon/BN/MI-SiC composite and a fast burner rig flame. Matrix processing of these composites by melt infiltration is carried out around 1450°C (the lowest temperature for this process being set by the melting point of silicon or its alloy). It has been shown that at those temperatures an ultrathin layer of carbon forms as a skin (~5-10 nm thick) on the Hi-Nicalon fiber regardless of whether it is an isolated filament[17], or embedded in a matrix.[18,19] Our

attempts to detect such a carbon layer in our starting material, between the fiber and interphase, was unsuccessful. The failure may be attributed to the resolution limitation of our TEM, however. It is reasonable to assume the existence of a carbon sublayer in our samples because the matrix processing condition for our samples are right for its formation. The presence of such a layer would explain the thorough penetration of degradation observed in our burner rig samples.

Figure 8(a) is a schematic diagram illustrating the formation of annular pores around a Hi-Nicalon fiber separated from its sheath of BN interphase by a much thinner C sublayer. At 800°C, elimination of the C sublayer through the reaction:

$$2C(s) + O_2(g) = 2CO(g) \qquad (3)$$

is much faster than conversion of the BN layer through eq. (1), with the result that the rate of recession of the C layer from the exposed surface is much greater than that of the BN layer, as shown in the diagram. The recession rate of carbon layers in such a situation has been the subject of recent investigations.[20,21] In experiments with 33-μm carbon cores in SCS-6 SiC fiber, from which they extrapolated for expected results for a 1-μm carbon interphase layer in a SiC-C-SiC composite, Eckel et al.[20] showed that if conditions are right for the rapid ingress of oxidants into the pore formed by carbon recession and the egress of CO therefrom, the process is only limited by the reaction rate (rather than by diffusion rate). Hence, the carbon layer may be eliminated very rapidly: in about 40 hours at 800°C a tube of carbon embedded in SiC may recede to a depth that is three orders of

magnitude greater than its thickness. Also, Windisch et al.[21] have determined, both from calculations and experimental measurement, the consumption rates of a 1.0-μm carbon interphase in a SiC-SiC composite oxidized in a TGA with different O_2-Ar mixtures at various temperatures. The calculated consumption rates agreed with their measured recession rates and with the extrapolations of Eckel et al.[20]

From those results we note that removal of the carbon layer in a SiC-SiC composite can leave behind open annular pores that extend deeper than the distances between fibers in our composite, in agreement with our observations. That situation, depicted in Figure 8(a), exposes the BN layer to ambient attack over the large surface area of the annular trench formed rather than over the narrow cross section that is normal to the fiber axis. In other words, the BN layer is effectively "undermined" through the much faster elimination of its adjoining C layer.

Figures 8(b) and (c) are schematic diagrams showing two adjacent fibers, and the effect of the formation of a borosilicate liquid around each of them. If the fibers are in close enough proximity, the net result is the dissolution of the walls of BN interphase and SiC cladding between them, so that the two fibers are now joined by a rigid bridge of silica (eventually) in the manner seen in Figure 6. From the high volume fraction of fibers in these materials (38-39%) it is easily shown that the greatest separation achievable between fibers through uniform distribution is about 3.2 μm. Given the difficulty of uniform infiltration of the BN interphase and SiC cladding during processing, achievable separation of fibers must be significantly less. Hence, neck contact between fibers is so prevalent as to be the rule

rather than the exception (Figure 5). That makes for easy embrittlement of the composite by the mechanism described here. The reactions involved in the interphase degradation process generate large amounts of gas (HBO_2, H_3BO_3, CO, NO, etc.) which can only exit by bubbling through the borosilicate glass produced. This is thought to be the cause of the ubiquitous pin holes depicted in Figure 8(c) and shown in Figures 5 and 6. The increasing viscosity of the glass, as it loses boron by hydrolysis, causes the glass and the holes to freeze in place. Note that, while the attack of oxidants may thin down the BN layer all around the fiber, it is only at the neck that "spot welding" of the fiber results because, elsewhere around the fiber, a sufficient thickness of the BN remains to permit the desired interphase compliance and debond. The significant and deleterious result of such a spot-welding effect has been demonstrated by Glime et al[5] with SiC-SiC microcomposites comprised of SCS-0 monofilaments in CVD SiC sheath with an interphase of CVD C. Oxidation of the microcomposites (made with long segments of the fiber sticking out at both ends) caused spot welding, by SiO_2, at the spots where the fiber exited the sheath. They found that fiber failure always occurred at the welds, and at stresses averaging four times lower than the baseline fiber strength. Furthermore, after dissolving the welds with HF solution they observed that the fibers regained their original baseline strengths.

4.4 Degredation in the Burner Rig

The foregoing analysis is consistent; yet it does not explain why severe degradation, by deep penetration of oxidants into the material, was observed in the burner rig but not in the furnace samples. The difference must lie in the very high oxidant flow rates achieved in the burner rig. The extent of penetration suggested by Figures 5 and 6 is noteworthy.

Figure 9 is a schematic diagram of our samples showing the orientation of fibers with respect to the burner rig flame. The flame impinged on the exposed ends of the [90°] fibers at the machined edge of the sample (shaded in the figure); yet the fibers seen in Figures 5 and 6 are [0°] fibers, which run up and down in the figure. That is to say, interphase damage propagated all the way down the [90°] fibers and across to the [0°] fibers. This requires carbon recession distances in the neighborhood of inches (tens of millimeters) or so down fibers in the sample hot zone. (Propagation of recession from the [90°] to the [0°] fibers also requires a connectivity of the interphase in those two directions; this is made possible by the same difficulty of uniform infiltration of the CVI SiC layer which is supposed to isolate each BN layer.) Extrapolation from the empirical results of Eckel et al.[19] leads us to expect only tens of micometers of carbon recession from the flame edge, and that is in agreement with the recession distances measured in our furnace samples (where oxidant flow velocities were low).

It should be pointed out that the calculations of Eckel et al.[20] and of Windisch et al.[21] are valid only for equilibrium conditions in a pore. Eckel et al.[20] showed that for a very thin vein of carbon, such as the sublayer suspected in our samples, the consumption process may undergo a transition from reaction-limitation (which is fast) to diffusion-limitation (which is slow). The transition is attributed to the "Knudsen effect" in which gas diffusion down the pore is controlled by molecule-to-wall collision rather than inter-molecular collision. (At 5-10 nm, the trench formed by removal of our carbon sublayer is only a few molecular distances wide, so that the Knudsen effect is applicable.) The inference is that the huge recession distances observed in our burner rig samples are not achievable under

the equilibrium conditions of a furnace oxidation. In contrast, the Mach 0.3 (100 M/s) flame velocity of our burner rig is probably adequate to propel the oxidants deep into the recession trench. This velocity factor is quite important (as manifested in its dramatic effect in our burner rig samples). Opila and Hann[22] have shown that the removal of SiC from a flat surface by the laminar flow of oxidant (a H_2O/O_2 mix) obeys the relationship:

$$k_l \quad \propto \quad V^{1/2}P_{ox}^{\ 2}/P_t \qquad (4)$$

where k_l is the linear recession rate of the SiC surface, V the oxidant flow velocity, P_{ox} the oxidant partial pressure, and P_t the total pressure. (Jacobson[23] found that the same relationship holds for the recession of a BN surface under the same oxidants and flow conditions.) While it would be simplistic to apply the analysis of Opila and Hann to the submicron confines of the trench from which C is being removed in our sample, especially in view of the turbulent flow conditions expected at Mach 0.3, an order-of-magnitude comparison is reasonable. Eq. (4) suggests that in going from the 0.5 cm/s rate of oxidant flow in our tube furnace to the 10,000 cm/s flow rate in our burner rig, material removal rate should increase by two orders of magnitude. This would explain why we observed severe degradation in the burner rig samples but not in the furnace samples.

5.0 Summary

Studies of SiC/BN/SiC bars exposed to oxidation by moist-to-wet air or oxygen for periods up to 500 hours at 800°C, in furnaces and in an atmospheric-pressure burner rig, have shown that:

1. The material undergoes insignificant degradation of its mechanical properties (strength and fracture strain) after exposures for up to 500 hours in an oxidant that is 30% H_2O + 70% O_2, or 150 hours in a 90% H_2O + 10% O_2 mix.
2. However, in a 100-150H exposure to the fast flame of a burner rig containing 10% moisture, the material loses over 60% of its strength and 90% of its fracture strain.
3. While moisture plays a key role in the mechanism of degradation at 800°C, the very fast flame speed in the burner rig greatly facilitates the deep ambient penetration of the material which leads to the severe damage observed in the burner rig samples.
4. Microstructural evidence of damage includes brittle bridges of silica which weld adjacent fibers together, causing stress concentrations and fiber failure; fracture mirrors indicative of fiber failure at the locality of the weld; and ubiquitous pin holes about the silica necks between fibers.
5. The glass bridge results from oxidation of the BN interphase to form liquid boria; dissolution of SiC by the boria to form liquid borosilicate; loss of boron from the borosilicate through volatilization by hydrolysis with the ambient moisture, leading to increasing viscosity and final rigidification of the glass.
6. Evidence of damage in the burner rig occurs all over the volume of material in the flame zone, indicating a connectivity of pathways for rapid ambient penetration of the samples.
7. The foregoing are consistent with the existence of a thin sublayer of carbon between interphase and fiber, which has been reported to form during matrix incorporation by melt infiltration in the Hi-Nicalon/CVI-BN/MI-SiC composites.

6.0 Conclusion

In the pesting temperature regime around ~800°C, the service conditions of a turbine engine (which include the unavoidable combination of ambient moisture and high flame speeds) carry a high potential for the severe degradation of mechanical properties in combustor components made of Hi-Nicalon/BN/MI-SiC, owing to the apparent existence in that material of an intrinsic pathway for rapid and deep penetration by the ambient.

6.0 Acknowledgment

The burner rig tests were performed by Mike .D. Cuy, and the mechanical tests by John Z. Gyekenyesi (both of the NASA Lewis Researc center); their assistance is appreciated. The author is also grateful to Greg Morscher (of NASA Lewis Research Center) for his ideas which stimulated much of the work done in this study.

7.0 References

1. M.W. Chase, Jr., C.A. Davies, J.R. Downey, Jr., D.J. Frurip, R.A. MacDonald, and A.N. Syverud, JANAF Thermochemical Tables (3rd Ed.), Am. Chem. Soc. & Am. Phys. Soc., New York, 1986.

2. T.J. Rockett, and W.R. Foster, "Phase relations in the System Boron Oxide - Silica", J. Am. Cer. Soc., 48 [2] (1965) 75-80

3. N.S. Jacobson, S. Farmer, A. Moore, and H. Sayir, "High Temperature Oxidation of Boron Nitride, Part I - Monolithic BN" (submitted to J. Am. Cer. Soc.)

4. N. S. Jacobson, G. Morscher, D.R. Bryant, and R.E. Tressler, "High Temperature Oxidation of Boron Nitride, Part II - BN Layers in Composites (id.)

5. W.H. Glime and J.D. Cawley, "Stress Concentration Due to Fiber-Matrix Fusion in Ceramic Matrix Composites," (submitted to J. Am. Ceram. Soc.)

6. F.E. Heredia, J.C. McNulty, F.W. Zok, and A.G. Evans, "Oxidation Embrittlement Probe for Ceramic-Matrix Composites", J. Am. Cer. Soc., 78[8](1995) 2097-2100

7. H.C. Cao, E. Bischoff, O. Sbaizero, M. Ruhle, A.G. Evans, D.B. Marshall, and J.J. Brennan, "Effect of Interfaces on the Properties of Fiber-reinforced Ceramics", J. Am. Cer. Soc., 73 [6] (1990) 1691-99

8. A.G. Evans, F.W. Zok, R.M. McMeeking, and Z.Z. Du, "Models of High-Temperature, Environmentally-Assisted Embrittlement in Ceramic-Matrix Composites", J. Am. Cer. Soc., 79 [9] (1996) 2345-52

9. G.N. Morscher, "Tensile Stress-Rupture of SiC_f/SiC_m Minicomposites with C and BN Interphases at Elevated Temperatures in Air" (submitted to J. Am. Cer. Soc.)

10. G.N. Morscher, D.R. Bryant, and R.E. Tressler, "Environmental Durability of BN-Based Interphases (for SiC_f-SiC_m Composites) in H_2O-Containing Atmospheres at Intermediate temperatures"; pp. 525-34 in Ceram. Eng. & Sci. Proc., 18 [3](1997)

11. L.U. Ogbuji, unpublished work

12. D.S. Fox, "Burner Rig Oxidation of Continuous Carbon Fiber Reinforced Silicon Carbide", pp. 553-64 in Advances in Ceramic-Matrix Composites, N.P. Bansal ed., Am. Cer. Soc., Westerville, OH 1993

13. N.S. Jacobson, "Corrosion of Silicon-Based Ceramics in Combustion Environments", J. Am. Cer. Soc., 76 [1] (1993) 3-28

14. L. Filipuzzi and R. Naslain, "Oxidation Kinetics of SiC Deposited from CH_3SiCl_3/H_2 Under CVI Conditions", J. Mater. Sci., 27 (1992) 3330-3334

15. E.Y. Sun, H-T. Lin, and J.J. Brennan, "Intermediate-Temperature Effects on Boron Nitride-Coated Silicon Carbide-Fiber-Reinforced Glass-Ceramic Composites, J. Am. Ceram. Soc., 80 [3] 609-14 (1997)

16. B.W. Sheldon, E.Y. Sun, S.R. Nutt, and J.J. Brennan, "Oxidation of BN-Coated SiC Fibers in Ceramic-Matrix Composites", J. Am. Cer. Soc., 79 [2] (1996) 539-43

17. G. Chollon, R. Pailler, R. Naslain, F. Laanani, M. Monthioux, and P. Olry, "Thermal Stability of a PCS-Derived SiC Fibre with a Low Oxygen Content (Hi-Nicalon)", J. Mater. Sci., 32 [2] (1997) 327-47

18. E.Y. Sun, S.R. Nutt, and J.J. Brennan, "Interfacial Microstructure and Chemistry of SiC/BN Dual-Coated Nicalon-Fiber-Reinforced Glass-Ceramic-Matrix Composites", J. Am. Cer. Soc., 77 [5] (1994) 1329-39

19. J.J. Brennan, S.R. Nutt, and E.Y. Sun, "Interfacial Microstructure and Stability of BN-Coated Nicalon Fiber/Glass-Ceramic Matrix Composites", pp. 53-64 in Ceramic Trans., vol. 58; A.G. Evans and R. Naslain, eds., Am. Cer. Soc., Westerville OH 199

20. A.J. Eckel and J.D. Cawley, "Oxidation Kinetics of a Continuous Carbon Phase in a Nonreactive Matrix", J. Am. Cer. Soc., 78 [4] (1995) 972-80

21. C.F. Windisch, C.H. henager, G.D. Springer, and R.H. Jones, "Oxidation of the carbon Interface in Nicalon-Fiber-Reinforced Silicon Carbide Composite," J. Am. Ceram. Soc., 80 [3] 569-74 (1997)

22. E.J. Opila and R.E. Hann, Jr., "Paralinear Oxidation of CVD SiC in Water Vapor", J. Am. Cer. Soc., 80 [1] (1997) 197-205

23. N.S. Jacobson, unpublished work

FIGURE CAPTIONS

Fig. 1 Schematic cross-sectional diagram of the SiC-SiC composite, illustrating degradation in a static ambient. Damage initiates at the surface and progresses inward, tow-by-tow.

Fig. 2 A chart of residual strength of SiC-SiC bars: as received (# 1), and following oxidation at 800°C in room ambient (#s 2,3) or in 30%H_2O+70%O_2 to 90%H_2O+10%O_2 (#s 4-8), or in a Mach 0.3 burner rig (#s 9-12). Only the burner rig caused significant loss of strength.

Fig. 3 A chart of the same results as residual strength versus ambient moisture content. Again, the only significant strength loss occurred in the burner rig (10% moisture).

Fig. 4 SEM fractographs of SiC-SiC samples oxidized in a tube furnace at 800oC: (a) 500H in 30% H_2O, and (b) 90% H_2O (balance O_2). Profuse fiber pull-out, millimeters long, indicate minimal degradation of interfacial properties.

Fig. 5 SEM fractographs of SiC-SiC composite oxidized in the burner rig at 800°C: (a) at lower magnification; (b) at higher magnification, showing pin holes between adjacent fibers.

Fig. 6 SEM fractographs of a burner rig SiC-SiC sample showing interphase degradation in the neck region between fibers. Arrows in (a) indicate slivers of glass formed next to the fibers, while those in (b) indicate fiber fracture initiation sites associated with the glass.

Fig. 7 EDS/SEM spectra from the interphase layer of SiC-SiC composite oxidized for 150 H at 800°C in the burner rig: (a) from the side of a fiber farthest from inter-fiber neck, and (b) from the segment of interphase between the pin holes at inter-fiber necks.

Fig. 8 Schematic cross sections through a SiC-SiC composite illustrating: (a) the BN interphase and suspected carbon sublayer next to the fiber, both layers recessed by ambient attack; (b) conversion of the C to glass; and (c) consequent bridging of the fibers by the glass.

Fig. 9 Schematic diagram of SiC-SiC bar showing fiber orientation during burner rig oxidation and illustrating the occurrence of interphase recession across fiber orientations.

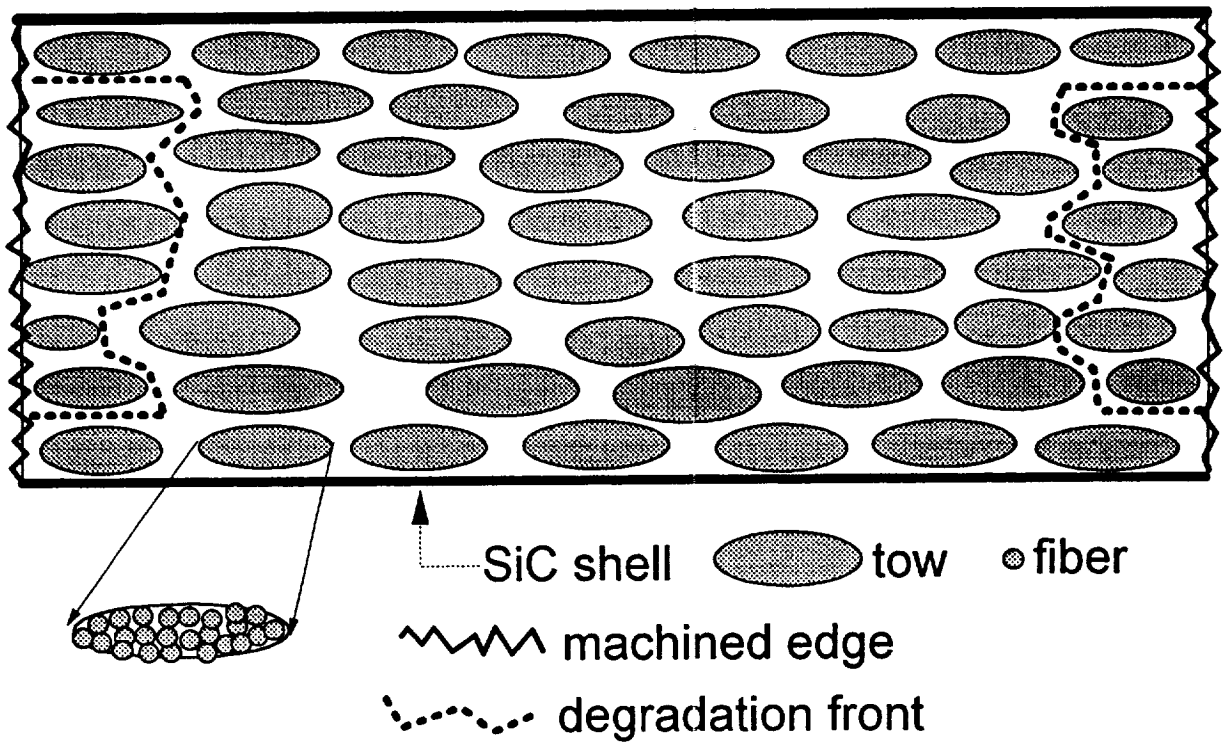

Fig. 1 Schematic diagram illustrating the inward advance of environmental degradation, one tow at a time, expected (and often observed) in SiC-SiC composites.

Table 1. Oxidation at 800°C and Post Testing of SiC-SiC Samples

#	Media[a] [Oxidant]	% H_2O	Velocity (M/s)	Time (H)	σ_u (MPa)	ε_f (%)	Failure Locus[b]
1	As Received				337	0.79	inside
2	BF [Air]	2.0[c]	~0.0	50	348	0.69	outside
3	BF [Air]	2.0	~0.0	400	341	0.79	inside
4	TF [O_2, H_2O]	30	0.005	500	385	0.72	outside
5	TF [O_2, H_2O]	60	0.005	50	342	0.86	outside
6	TF [O_2, H_2O]	60	0.005	150	388	0.82	inside
7	TF [O_2, H_2O]	90	0.005	150	376	0.83	inside
8	TF [O_2, H_2O]	90	0.005	150	365	0.81	outside
9	BR [O_2, H_2O][d]	10	100	150	148	0.08	outside
10	BR [O_2, H_2O][e]	10	100	120	135	0.07	inside
11	BR [O_2, H_2O][d]	10	100	150	155	0.11	outside
12	BR[O_2, H2O][e]	10	100	150	110	0.59	inside

(a) BF = box furnace, TF = tube furnace, BR = burner rig
(b) Relative to gage zone (which coincided with the BR oxidation hot zone)
(c) Average of diurnal oscillations
(40-98% Rel. Humidity, 49-71°F; 07/25/96-08/18/96)
(d) The Flame impinged on edge of sample (at exposed fiber ends)
(e) The Flame impinged on the sealed surface of the sample.

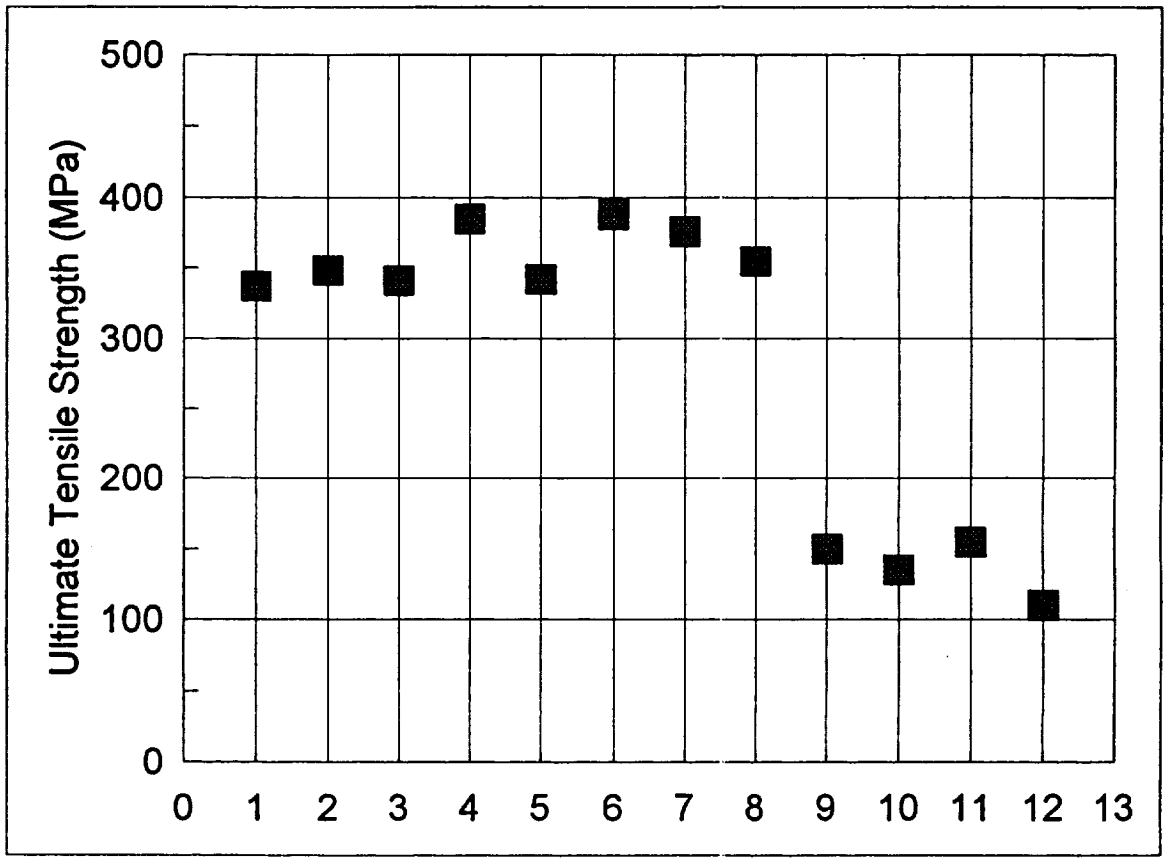
Ultimate Tensile Strength (MPa)
500
400
300
200
100
0
0 1 2 3 4 5 6 7 8 9 10 11 12 13

Specimen No.

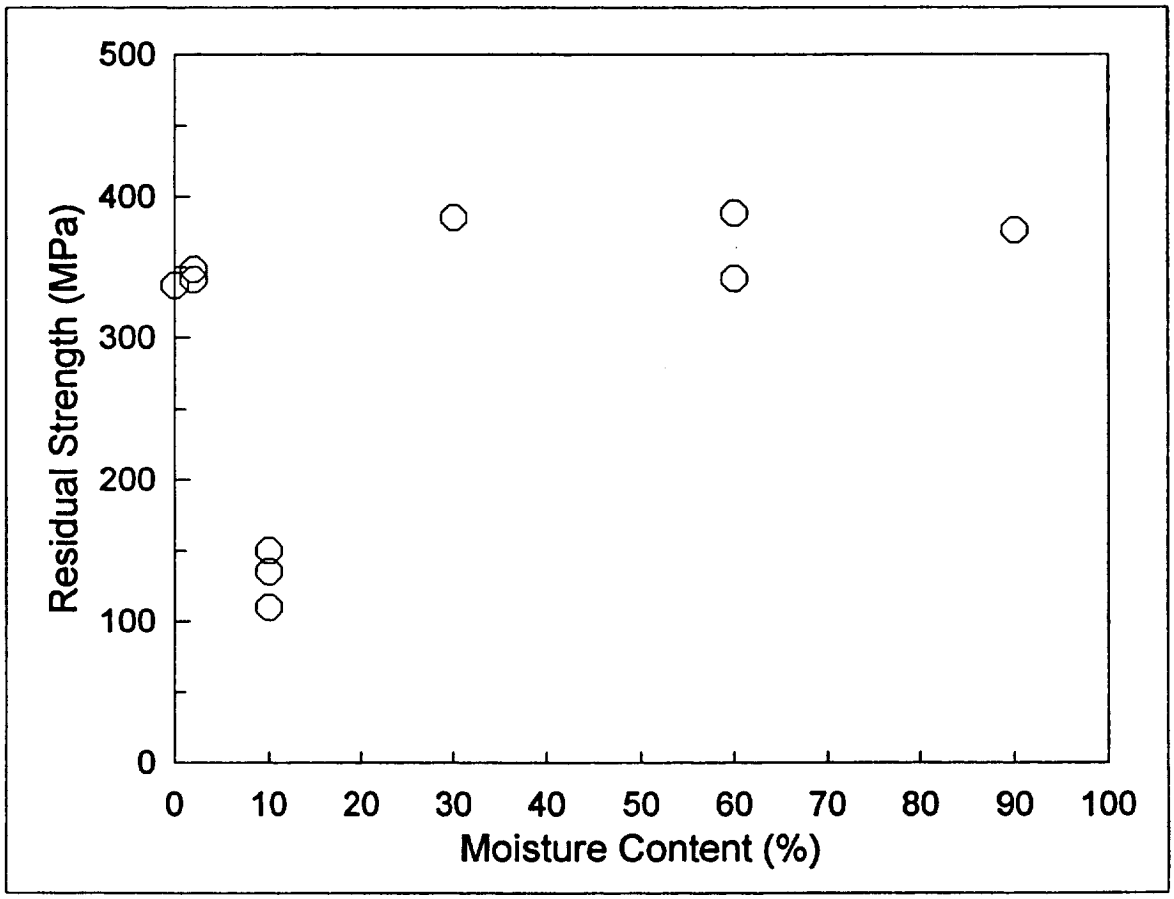
Residual Strength (MPa)
500
400
300
200
100
0
0
10
20
30
40
50
60
70
80
90
100
Moisture Content (%)